


Temperature and Ultrasound-Responsive Nanoassemblies for Enhanced Organ Targeting and Reduced Cardiac Toxicity

Mingzhou Jiang^{1,*}, Yiming Wang^{2,*}, Jinjin Zhang^{2,*}, Xi Fan¹, Milayi Jieensi¹, Fang Ding², Yiqing Wang¹, Xiaotian Sun¹ 

¹Department of Cardiothoracic Surgery, Huashan Hospital of Fudan University, Shanghai, People's Republic of China; ²Department of Cardiology, Huashan Hospital of Fudan University, Shanghai, People's Republic of China

*These authors contributed equally to this work

Correspondence: Yiqing Wang; Xiaotian Sun, Department of Cardiothoracic Surgery, Huashan Hospital of Fudan University, 12 Wulumuqi Road, Shanghai, 200040, People's Republic of China, Email wangyiqing@huashan.org.cn; drsunxiaotian@126.com

Background: Biocompatible nanocarriers are widely employed as drug-delivery vehicles for treatment. Nevertheless, indiscriminate drug release, insufficient organ-specific targeting, and systemic toxicity hamper nanocarrier effectiveness. Stimuli-responsive nano-sized drug delivery systems (DDS) are an important strategy for enhancing drug delivery efficiency and reducing unexpected drug release.

Methods: This study introduces a temperature- and ultrasound-responsive nano-DDS in which the copolymer p-(MEO₂MA-co-THPMA) is grafted onto mesoporous iron oxide nanoparticles (MIONs) to construct an MPL-p nano-DDS. The copolymer acts as a nanopore gatekeeper, assuming an open conformation at sub-physiological temperatures that allows drug encapsulation and a closed conformation at physiological temperatures that prevents unexpected drug release during circulation. Lactoferrin was conjugated to the nanoparticle surface via polyethylene glycol to gain organ-targeting ability. External ultrasonic irradiation of the nanoparticles in the targeted organs caused a conformational change of the copolymer and reopened the pores, facilitating controlled drug release.

Results: MPL-p exhibited excellent biocompatibility and rare drug release in circulation. When targeting delivery to the brain, ultrasound promoted the release of the loaded drugs in the brain without accumulation in other organs, avoiding the related adverse reactions, specifically those affecting the heart.

Conclusion: This study established a novel temperature- and ultrasound-responsive DDS that reduced systemic adverse reactions compared with traditional DDS, especially in the heart, and demonstrated excellent organ delivery efficiency.

Keywords: temperature- and ultrasound-responsive, systemic toxicity, mesoporous iron oxide nanoparticles, drug delivery

Introduction

Nanoparticle composite materials have been widely used for medication delivery throughout the last decade.¹ However, common nanocomposites cannot control drug release in circulation, resulting in a lack of organ targeting with limited organ therapeutic effects.^{2,3} Furthermore, drug release in the bloodstream can increase the risk of toxicity in non-targeted organs, such as by causing heart damage.⁴ Therefore, there is a critical need to develop an intelligent drug delivery system (DDS) with limited circulatory release and controlled release in the targeted organs.

Mesoporous iron oxide nanoparticles (MIONs) nanocarriers demonstrate important advantages given their high load capacity and large surface area. However, the drugs loaded within the nanoparticles freely traverse the mesoporous channels, resulting in an uncontrolled drug during circulation. Accordingly, equipping the surface nanoparticles with functional groups that can react to external stimuli and facilitate controlled drug release has been explored.⁵ Such functional groups greatly enhance DDS specificity and efficiency in therapeutic applications.

In this study, we engineered the MION surface with a suite of organic ligands that facilitated controlled drug release with temperature and ultrasonic stimulation. Organisms naturally provide physiological temperature conditions, while ultrasound is cost-effective, easily implemented, and non-invasive.⁶ The temperature-responsive polymer 2-(2-methoxyethoxy) ethyl methacrylate [p-(MEO₂MA)] was used based on its temperature-reactive feature,^{7–9} one important characteristic of which is its lower critical solution temperatures (LCST): the hydrogen bond network of the polymer remains stable at temperatures below the LCST and forms bonds with water molecules to exhibit hydrophilic properties; when temperatures exceed the LCST, the polymers become hydrophobic as the hydrogen bonds are disrupted to close the nanopores.^{7,10,11} Grafting the p-(MEO₂MA) onto the DDS enables low-temperature drug loading into nanocomplexes with the open polymer conformation. Subsequently, the polymer-based nanogates close to restrict the drug inside the nanoparticles when physiological temperatures rise above the LCST after *in vivo* administration.¹²

The temperature-sensitive properties of nanoparticles were utilized by several research.^{11,12} However, previous designs that relying on temperature properties often struggle to smartly control both the timing and location of drug release in the *in vivo* models. For precisely controlled drug release, 2-tetrahydropyranyl-methacrylate (THPMA) was combined with the p-(MEO₂MA) to reopen the nanopores in response to external ultrasonic stimulation. When the nanoparticles reach the targeted organs, ultrasonic irradiation cleaves the hydrophobic tetrahydropyranyl moieties in the polymer structure, opening the nanogates for drug release.^{13,14} Therefore, the drug can be precisely released in specific organs under ultrasonic stimulation, avoiding obvious systemic adverse effects.

To enhance the targeting capability of the delivery system in specific organs, lactoferrin (LF) was conjugated with polyethylene glycol (PEG) onto the nanoparticle surface to confer organ-targeting ability, which aids drug crossing of the blood–brain barrier (BBB) through the LF receptor and central nervous system (CNS) targeting.¹⁵ Furthermore, PEG prolongs the nanoparticle circulation time, mitigating immune system phagocytosis, including the reticuloendothelial system (RES) and mononuclear phagocytic system, ensuring sufficient effecting time.^{16–20} While Grafted PEG can improve the stability of nanoparticles in circulation, thereby enhancing the drug delivery efficacy.^{21,22}

In this study, we developed a novel DDS termed MION-PEG-LF-p-(MEO₂MA-*co*-THPMA), abbreviated to MPL-p. The MPL-p temperature-sensitive nanogates allow drug encapsulation and safe transport to specific organs at physiological temperatures. Then, the nanocarriers release their cargo upon external ultrasonic stimulation. The properties and advantages of MPL-p were evaluated using the cytotoxicity drug doxorubicin hydrochloride (DOX) as the loading drug (Figure 1). DOX accumulating in circulation or organs can result in dose-dependent tissue toxicity, including renal and gonadal toxicities.^{23–25} Furthermore, DOX administration has been associated with cardiac dysfunction, cardiomyopathy, and cardiac death.^{26–28} Therefore, we constructed a novel temperature- and ultrasound-responsive nano-DDS that can regulate *in vivo* drug release, enhance organ-targeting efficacy, and effectively reduce systemic toxicity.

Materials and Methods

Materials and Reagents

DOX and LF were obtained from Aladdin Chemical Co., Ltd. (Shanghai, China). 3-aminopropyltriethoxysilane (APTES), MEO₂MA, 4-Cyano-4-(thiobenzoylthio) pentanoic acid (CPADB), 2,2'-Azobis(2-methylpropionitrile) (AIBN), THPMA, 3-butylene acid, maleimide-polyethylene glycol-NHS (Mal-PEG-NHS), and N-succinimidyl-S-acetylthioacetate (SATA) were purchased from Sigma-Aldrich (St Louis, MO). All other reagents were of analytical grade and used as purchased. All solutions utilized Milli-Q water, and deaeration under an N₂ atmosphere was applied before the experiments. The detailed information on the experimental animals was described in the [Supplementary Material](#).

Characterization

Transmission electron microscopy (TEM) imaging was performed using a JEM-2100 (Hitachi, Tokyo, Japan) instrument operating at 75 kV, which was fitted with a CCD camera (KeenView Camera). The size distribution of the nanoparticles (NPs) was determined using dynamic light scattering (DLS) with a Mastersizer 2000 (Malvern Instruments Inc, UK). Furthermore, N₂ adsorption measurements were obtained using a Micromeritics ASAP 2010 instrument; the BET method was applied to the isotherm for surface area calculation, while the BJH method was utilized to determine the pore size

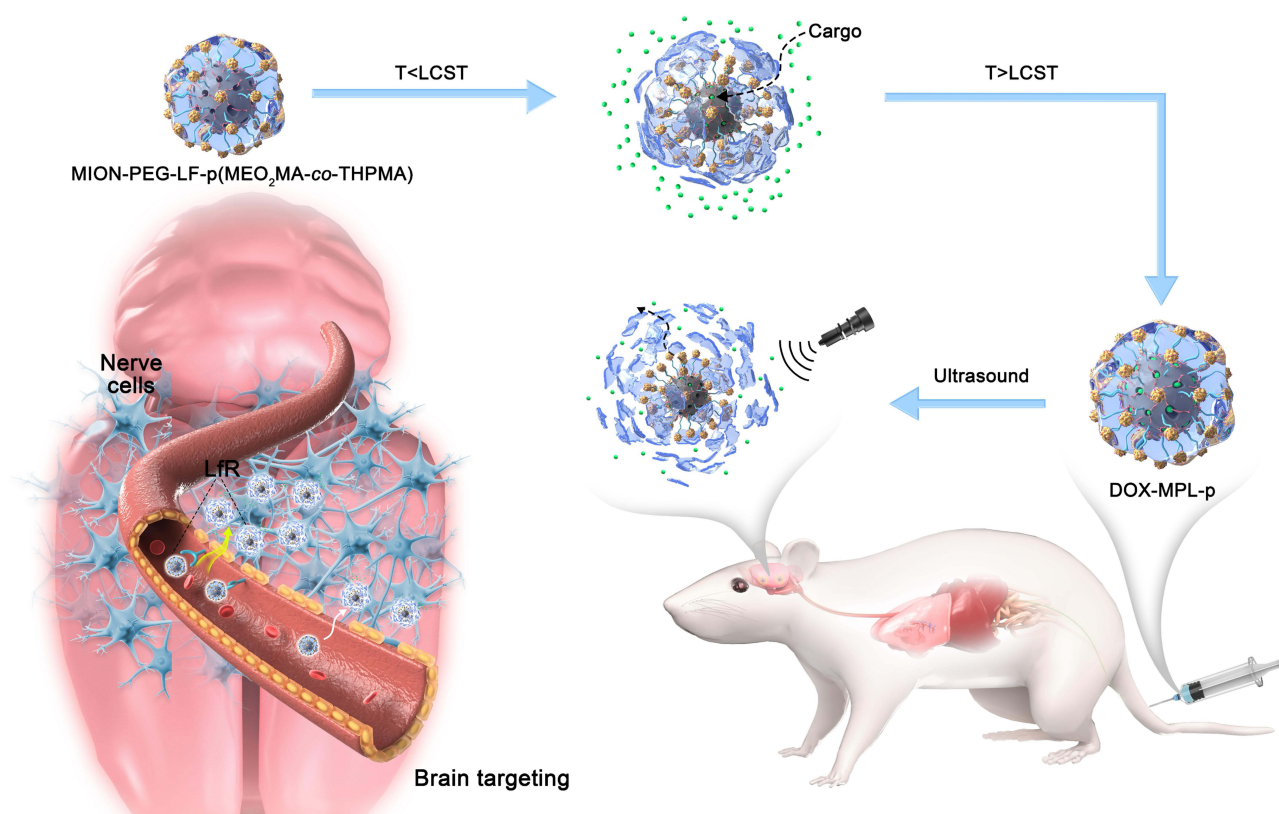


Figure 1 Synthesis and working schematic diagram of the novel brain-targeted nano ultrasound-controlled release system DOX-MPL-p. At temperatures below LCST, the drug is loaded into MPL-p. At temperatures higher than LCST, DOX-MPL-P blocks the drug and is injected intravenously into mice, limiting the release of DOX in the circulation. With LF, DOX-MPL-p targets the brain across BBB in a receptor-mediated mechanism and eventually disrupts to release of the drug upon ultrasonic stimulation.

distribution determination. The Fourier transform infrared (FTIR) spectra were acquired using a Nicolet (Thermo Fisher Scientific) Nexus spectrometer equipped with a Smart Golden Gate ATR accessory. The mesopore diameter was identified by the peak value in the pore size distribution curve. A Bruker spectrometer at 400 MHz was used to collect the ¹H-NMR spectra of p-(MEO₂MA-co-THPMA) in deuterated chloroform (CDCl₃). Fluorescence measurements were conducted using a Biotek Synergy 4 device, while fluorescence microscopy observations were made utilizing an Evos FL Cell Imaging System. Vacuum freeze-drying method was applied for measuring the nanoparticle weight, for the thermogravimetric analysis (TGA) method may cause the loss of the polymer structure (Figure S1). Differential scanning calorimetry (DSC) was employed to verify the temperature-sensitive properties of the constructed nanoparticles (Supplementary Materials).

Synthesis of MIONs

MIONs synthesis was conducted based on the previous method.²⁹ Initially, a mixture of styrene (9 mL) and methacrylic acid (1 mL) was dispersed in deionized (DI) water (70 mL) and heated to approximately 75 °C with continuous stirring for 30 mins. Then, potassium peroxydisulfate (0.1 g) dissolved in 10 mL of DI water was gradually added to the suspension above. The suspension was left to react at 75 °C for 24 h, and the resulting polystyrene nanoparticles were weighed and combined with ethylene glycol (30 mL) and additional DI water (170 mL). This mixture was then supplemented sequentially with potassium nitrate (0.111 g), ferrous chloride (0.446 g), and methenamine (2 g) before being heated at 80 °C for 3 h under N₂ protection. The resultant mixture was cooled to room temperature before centrifugation for nanoparticle collection. The nanoparticles were rinsed with DI water to eliminate the remaining reagents, followed by gradual heating up to 500 °C at a rate of 15 °C/min. The thermal reaction was extended for

3 h at the same temperature to facilitate iron oxidation. It was subsequently cooled to room temperature, resulting in the formation of MIONs.

Synthesis of p-(MEO₂MA-Co-THPMA)

The CPADB (10 mg), THPMA (94.5 mg), MEO₂MA (327 mg), and AIBN (1.77 mg) were used to synthesize p-(MEO₂MA-co-THPMA), and the process was modified by the previously method.¹³ The materials were added to a sealed vial, and the dioxane was used as the solvent. After it was stirred to dissolve, the mixture was frozen in liquid nitrogen, vacuumed with an oil pump, and dissolved in a water bath. Then the vial was placed in an oil bath at 70 °C for 20 h and frozen in liquid nitrogen. After returning to room temperature, the reaction liquid was added into a 10 mL centrifuge tube, and 9 mL of petroleum ether was added for sedimentation. The solution was subjected to centrifugation at 4000 rpm for 5 mins, followed by supernatant removal. Methylene chloride was employed as a solvent to dissolve the precipitate, while petroleum ether was utilized for solid settling. The copolymer p-(MEO₂MA-co-THPMA) was obtained after vacuum freeze-drying and characterized by ¹H NMR and FT-IR spectroscopy.

Synthesis of MION-PEG-LF

5 mg of MIONs was dispersed with 15 mL of DI water under the ultrasound for 5 mins. 2.5 mg of APTES was added to the HCL solution (PH 4.0) to react until it was no longer exothermic. The solution was mechanically stirred for 4 h under N₂ atmosphere protection at 65 °C, followed by being centrifuged at 8000 rpm and 4 °C for 10 mins. The supernatant was removed before being added to anhydrous ethanol and dispersed by the ultrasound. The solution was treated with N₂ for 30 mins, and 10 mg of Mal-PEG-NHS powder (MW 5000) was then added. The intermediate product Mal-PEG-MION was obtained after being stirred for 5 h.

5 mg of LF (5 mg) and 16.35 mg of SATA were dispersed into PBS and shaken for 1 h to activate LF. Then, the SATA-modified LF was reacted with 0.1 M hydroxylamine in an aqueous solution containing a sodium acetate buffer of about pH 7.0 for 2 h at room temperature. The solution was centrifuged at 12,000 rpm for 30 mins (10 kd ultrafiltration tube), and all supernatants were collected to remove the excess SATA. The solution was mixed with Mal-PEG-MION for maleimide coupling and agitated at 25 °C for 2 h. Impurities were subsequently removed using filters (0.45 μm), and vacuum lyophilization was used to obtain the resulting product MION-PEG-LF.

Synthesis of MION-PEG-LF- p-(MEO₂MA-Co-THPMA)

MION-PEG-LF (1 mg) and butanoic acid (50 μL) were utilized as feedstock for the attachment of vinyl groups onto the surface of MNP. The raw materials were diluted in 10 mL of DI water and subjected to ultrasonic dispersion for 15 mins, followed by incubation at 70 °C for 30 mins. Cetyltrimethylammonium bromide (CTAB, MW 364.46) was added to the solution (0.1 M) to enhance nanoparticle stability and minimize magnetic particle aggregation. Subsequently, the solution was centrifuged at 5000 rpm for 30 mins to remove the excess butanoic acid in the supernatant. After 10 mins of nitrogen blowing, the solution was heated to 70 °C under nitrogen protection before adding copolymer p-(MEO₂MA-co-THPMA) (128.5 mg) and triethylene-glycol-dimethacrylate (TEGDMA) (20.4 mg). The mixture was stirred under N₂ atmosphere for additional 15 mins, followed by introducing 2,2'-azobis[2-methylpropionamide] dihydrochloride (AAPH, 100 μL, 0.1 M) into the reaction. The stirring process was performed at 70 °C for 2 h before gradually being cooled to room temperature. The magnetic separation and purification steps were repeated 4 times before ultrasonic dispersion in water. Finally, the obtained product, MION-PEG-LF-p-(MEO₂MA-co-THPMA) (MPL-p), was filtered through a syringe filter (0.45 μm), followed by vacuum lyophilization.

Drug Loading to MPL-p

The drug-loading process was performed according to the previous method.³⁰ Briefly, DOX and MPL-p were mixed in DI water at 4 °C and stirred for 24 h until the drug was loaded into the mesoporous structure of MIONs. After magnetically separating DOX-loaded MPL-p at room temperature, the surplus drug was rinsed off with DI water. This process was repeated until DOX was no longer detected in the supernatant. DOX-MPL-p was then dried in a vacuum and weighed. For comparison, DOX-MION was synthesized using the similar method. The drug-loading content (DLC) and

drug-loading efficiency (DLE) were calculated from Equations 1 and 2. The methods for cytotoxicity testing of DOX-MPL-p in vivo and in vitro and drug release kinetics studies in vitro are described in detail in [Supplementary Material](#).

$$\text{DLC}(\text{wt}\%) = \frac{\text{amount of DOX in the MPL-p}}{\text{amount of MPL-p}} \times 100 \quad (1)$$

$$\text{DLE}(\text{wt}\%) = \frac{\text{amount of DOX in the MPL-p}}{\text{total amount of DOX}} \times 100 \quad (2)$$

In vivo Pharmacokinetic Studies

Mice were injected via the tail vein with DOX and DOX-MPL-p at the same dose of DOX (4 mg/kg). Blood samples were collected at intervals of 0min, 15mins, 30mins, 1h, 2h, 4h, 8h, 10h, and 24h after injection, and centrifuged to separate plasma. The plasma DOX concentrations were then quantified via a microplate reader utilizing a pre-established standard curve for calibration ([Supplementary Material](#)).

Evaluation of Survival and Heart Function

Each mouse was administered an equivalent dose of either free DOX or DOX-MPL-p, and the same volume of PBS was administered as Vehicle (each n = 8). After 4 h of administration, the DOX-MPL-p group underwent ultrasonic stimulation. Cardiac structure and function were evaluated at 2 w post administration utilizing Vevo 3100 echocardiography. Representative M-mode cardiac ultrasound images were identified. Stroke volume, ejection fraction (EF), and fractional shortening (FS) were calculated. Over a period of 30 d, survival rates were monitored and recorded.

Organ Targeting Assessment of DOX-MPL-p

To further evaluate the brain-targeting efficacy of MPL-p, the near-infrared fluorescent dye DiR was incorporated into the mesoporous structure of MPL-p, providing a fluorescent marker for the material. Briefly, a mixture of 1 mg DiR and 5 mg MPL-p was stirred at 4 °C for 2 h, followed by magnetic separation and PBS washing to eliminate unbound dye, yielding DiR@MPL-p. DiR@MION, was synthesized using an identical protocol as the control. Male C57 mice (n = 12) received tail vein injections of DiR@MPL-p or DiR@MION at a dosage of 10 mg/kg. After the injections at intervals of 0.5 h, 4 h, 8 h, and 24 h, the mice were humanely euthanized. Tissues from the brain, heart, liver, spleen, and kidney were harvested for analysis of fluorescence signals using the IVIS Lumina III Bioluminescence Imager for signal quantification.

In the ultrasound-affecting experiment, the mice received injections of DOX-MPL-p at a dosage of 10 mg/kg, and ultrasonic stimulation (1 MHz, 10 mins) was applied at 2 h, 4 h, and 8 h post-injection. The brain tissues were then dissected, and homogenized in methanol via high-speed agitation, followed by centrifugation at 12,000 rpm. The resulting supernatant was collected for DOX concentration analysis.

Immunofluorescence Study of Brain

Mice were anesthetized 24 h after drug administration with DiR@MPL-p or DiR@MION (10 mg/kg), followed by humane euthanasia. The harvested brain tissues were immediately fixed in 4% paraformaldehyde and processed into paraffin sections through dehydration and embedding. Antigen retrieval on the section surfaces was performed using a sodium citrate solution, followed by serial PBS washes to remove residual impurities. Neurofilament protein NF200 solution was applied for neuronal identification, while 4',6-diamidino-2-phenylindole (DAPI) staining was utilized to visualize cell nuclei at excitation and emission wavelengths of 466 nm and 504 nm, respectively. The sections were then examined under a fluorescence microscope (Leica Camera Co., Wetzlar, Germany) to detect the presence or absence of DiR signals (excitation wavelength 750 nm, emission wavelength 782 nm) in the brain tissues.

Statistical Analysis

All data were statistically analyzed using GraphPad Prism 8.0 software and SPSS Statistics Base 22.0 software, which were presented in the form of mean ± standard error (SEM). The Brown-Forsythe and Shapiro–Wilk tests were used to

test the normal distribution and variance. Group comparisons were conducted using a one-way analysis of variance (ANOVA), followed by a Student's *t*-test. Differences were deemed statistically significant when the P-value was less than 0.05. Furthermore, asterisks were used to illustrate the level of significance: (*) for $P < 0.05$, (**) for $P < 0.01$, and (***) for $P < 0.001$.

Results

Characterization

The MPL-p was successfully synthesized as expected (Figure 2). The TEM image illustrates the morphology of simple MION, which are characterized by their uniform size and regular geometric shape (Figure 3a). The MION pore size was 0–10 nm (Figure 3b). The BET-specific area was a typical representation of the mesoporous structure of the particle (Figure 3c). The BET-specific area was $97.7 \text{ m}^2/\text{g}$. After the MIONs were bound to the functional groups and loaded with drugs, the electron microscopy image of DOX-MPL-p confirmed the uniform polymer coating on the MION surface (Figure 3d). DLS assessment revealed that the DOX-MION particle size was between 170 and 180 nm, and that of DOX-MPL-p was 195–205 nm (Figure 3e and f). The two nanoparticle types remained stable after one-week dispersion in physiological saline (Figure 3g). The DOX-MPL-p PDI was 0.219 ± 0.07 . On average, the MION-PEG-LF weight was 1.39 times more than that of the MION, and the MPL-p weight was 1.24 times more than that of the MION-PEG-LF (Figure 3h). The MION DLC and DLE were $61.6\% \pm 3\%$ and $54.6\% \pm 6.4\%$, respectively, while those of MPL-p were $40.8\% \pm 4.3\%$ and $39.3\% \pm 4.8\%$, respectively. The successful loading of DOX into MPL-p was confirmed by recording the nanoparticle fluorescence spectra under excitation at 490 nm. Compared with free DOX, DOX-MPL-p exhibited fluorescence quenching at the same concentration and spectral characteristics, indicating successful drug encapsulation (Figure 3i).

The dual-responsive copolymer p-(MEO₂MA-co-THPMA) had a characteristic ¹H NMR spectrum, and the THP portion disappeared under ultrasonic stimulation (Figure 4a). The successful integration of MION with PEG, LF, and p-(MEO₂MA-co-THPMA) was confirmed using FT-IR: the successful attachment of PEG was confirmed by comparing the spectra between the MION and MION-PEG-LF within the 400–4000 cm⁻¹ range, which demonstrated the successful attachment of PEG (Figure 4b). The peak observed at 669 cm⁻¹ represented the C-S bond, demonstrating the conjugation

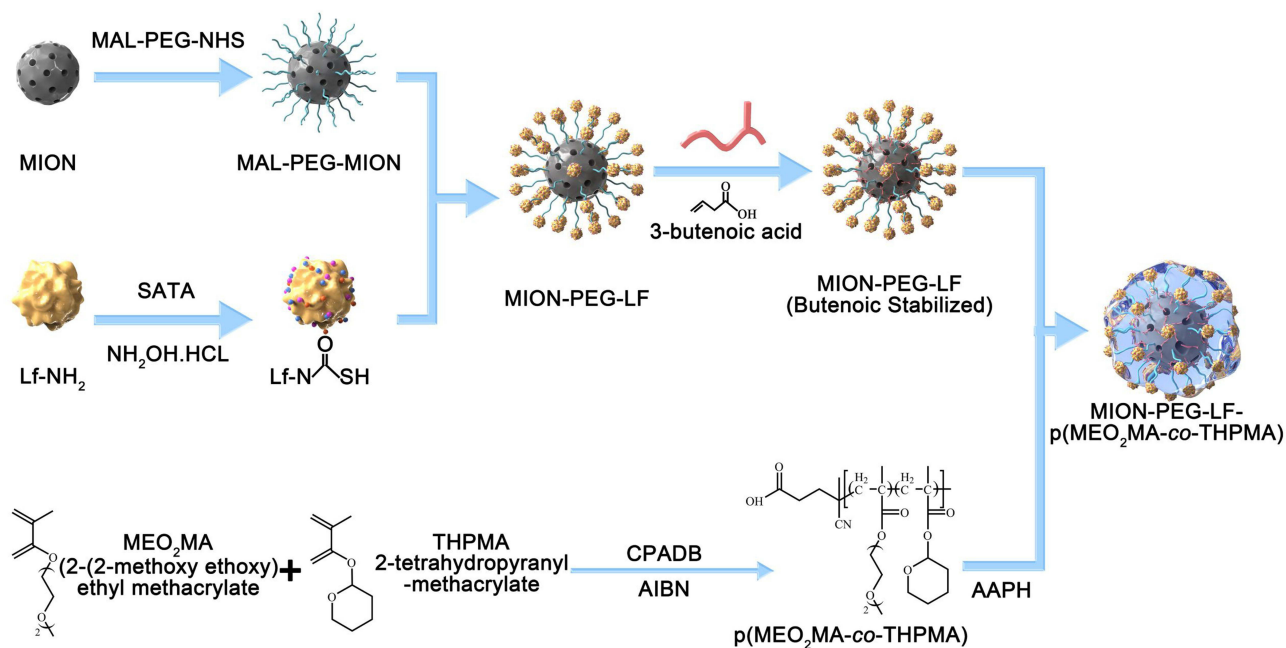


Figure 2 Procedures of synthesizing the MION-PEG-LF-p(MEO₂MA-co-THPMA). MIONs went through sequential conjugation with LF, Mal-PEG-NHS, and p(MEO₂MA-co-THPMA) to get MION-PEG-LF- p(MEO₂MA-co-THPMA), which was named as MPL-p.

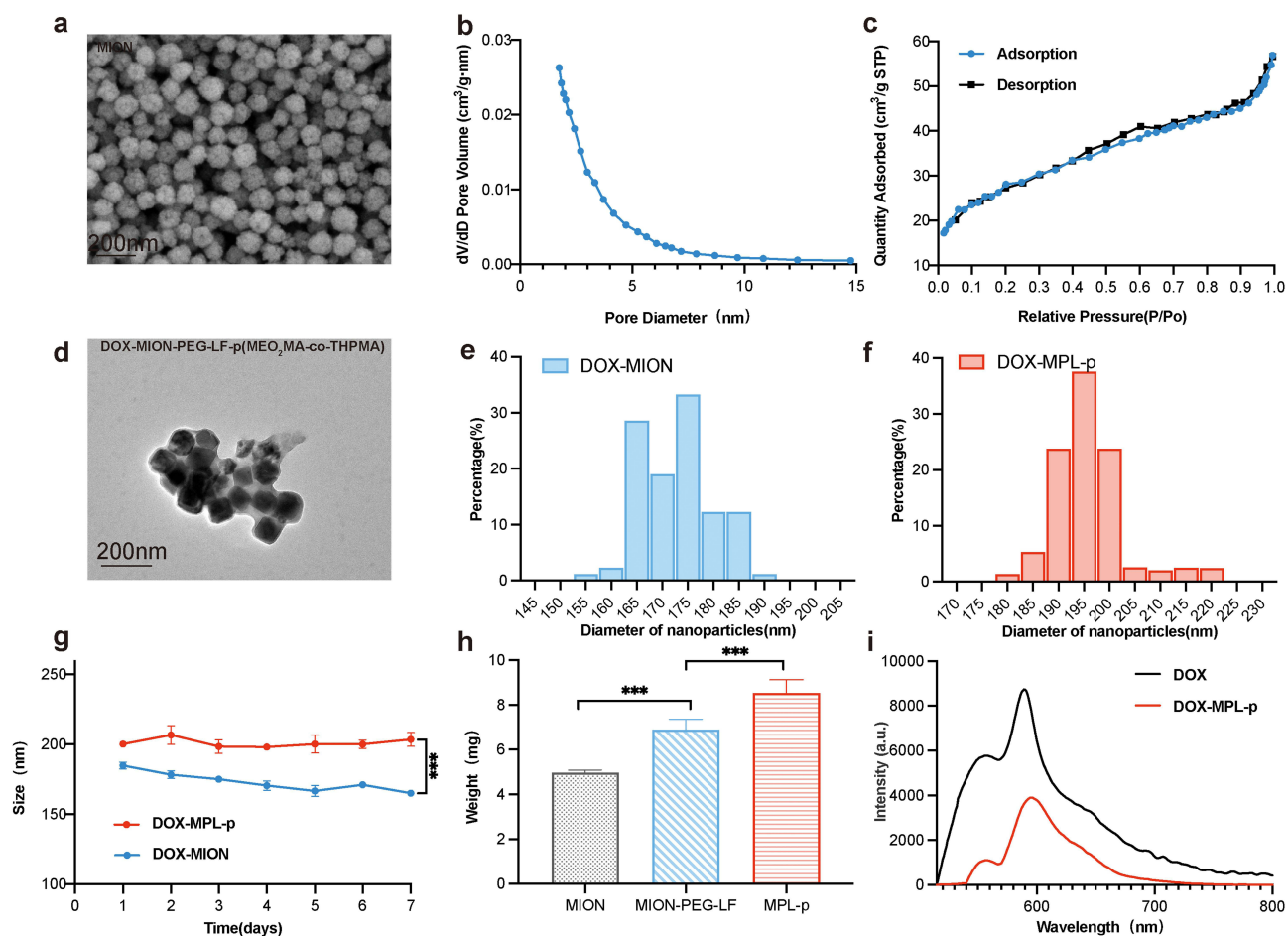


Figure 3 Characterization of MION-PEG-LF-p(MEO₂MA-co-THPMA) during synthesis and drug loading process. The TEM images of MION (a); (b) Pore size distribution of MION; (c) N₂ adsorption/desorption isotherm of MION; The TEM images of DOX-MPL-p (d); (e) The DLS results for DOX-MION; (f) The DLS results for DOX-MPL-p; (g) Stability of DOX-MION and DOX-MPL-p in physiological saline, n=3; (h) Comparison of average weight of MION, MION-PEG-LF and MPL-p, n=6; (i) Fluorescence spectra of DOX and DOX-MPL-p with a DOX concentration of 0.5 mg/mL. Asterisks were used to illustrate the level of significance: (***) for P < 0.001.

of the thiolate salt LF (Figure 4c). The copolymer p-(MEO₂MA-co-THPMA) exhibited a characteristic infrared spectrum (Figure 4d). The spectral comparison of MION-PEG-LF and MPL-p within the 400–4000 cm⁻¹ range confirmed the successful attachment of the copolymer, and a specific spectral band caused by the stretching vibration of Fe-O in iron oxide at 530 cm⁻¹ was observed (Figure 4b, c and e), proving that the iron oxide particles successfully wrapped the copolymer after being bounded to LF. The temperature-sensitive property of DOX-MPL-p was further verified by DSC method (Figure S2), exhibiting an endothermic effect of the nanoparticles around 37°C, which is caused by the collapse of polymers on the particle surface.

DOX Release Profile and Mechanistic Biological Evaluation

The dual-responsive drug release characteristics of MPL-p were validated using DOX, the concentration of which was determined using a standard curve (Figure S3). The in vitro experiments revealed that the drug release from DOX-MION was not significantly temperature-dependent. The drug release of DOX-MPL-p was limited within 48 h at 37 °C, comparing with a release increasing at 4 °C when the copolymers on the particle surface were hydrophobic (Figure 5a). Under ultrasonic stimulation at 37 °C, DOX-MPL-p efficiently release DOX, with the final amounts close to DOX-MION without polymer modification (Figure 5b). Under the same stimulus duration (10 min), the ultrasonic effect at 1 MHz was superior to that at 50 and 25 kHz. However, no obvious increase in drug release was observed at 2 MHz compared to 1 MHz (Figure 5c). Consequently, we selected the 1 MHz frequency for subsequent experiments.

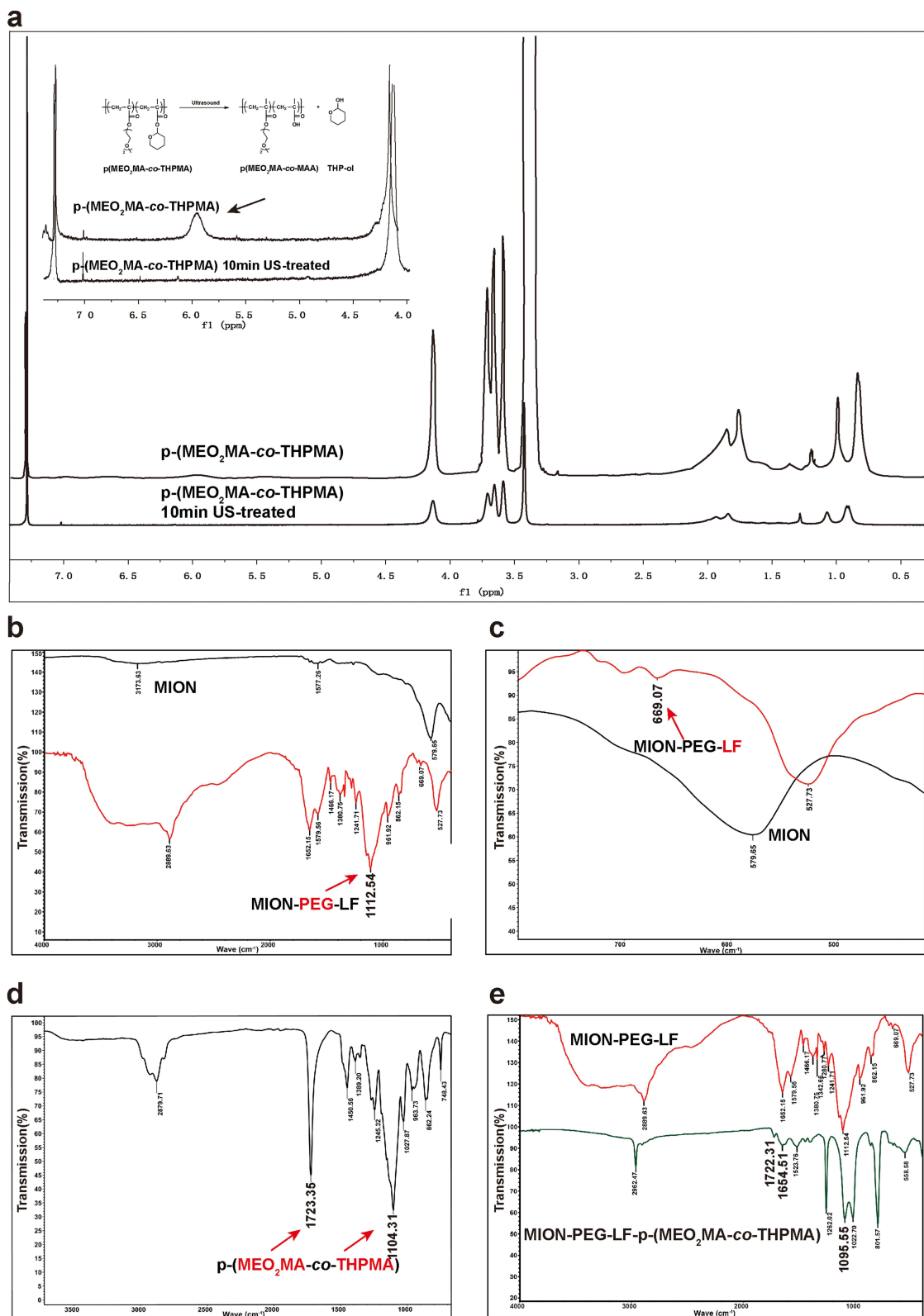


Figure 4 Characterization of MION-PEG-LF-p(MEO₂MA-co-THPMA). (a) ¹H NMR spectra of p(MEO₂MA-co-THPMA) before and after ultrasound treated for 10min, 1 MHz, 100W; (b) Compare the infrared spectra of MION and MION-PEG-LF in the range of 400–4000 cm⁻¹. The vibration of C-O in PEG alcohol molecules was observed at 1100 cm⁻¹; (c) Compare the infrared spectra of MION and MION-PEG-LF in the range of 400–800 cm⁻¹. The typical C-S bond in MION-PEG-LF was observed at 669 cm⁻¹, which is evidence of the conjugation of thiolated LF; (d) The infrared spectrum of the copolymer p(MEO₂MA-co-THPMA) shows a characteristic peak of THPMA at 1104 cm⁻¹ and a characteristic peak of MEO₂MA at 1723 cm⁻¹; (e) Compare the infrared spectra of MION-PEG-LF and MION-PEG-LF-p(MEO₂MA-co-THPMA) in the range of 400–4000 cm⁻¹. The vibration of C-O in PEG alcohol molecules and the characteristic peak of THPMA were observed at 1100 cm⁻¹, the characteristic peak of MEO₂MA was observed at 1722 cm⁻¹, and the vinyl functional group on MION was observed at 1650 cm⁻¹, which is the key group for connecting the copolymer to MION.

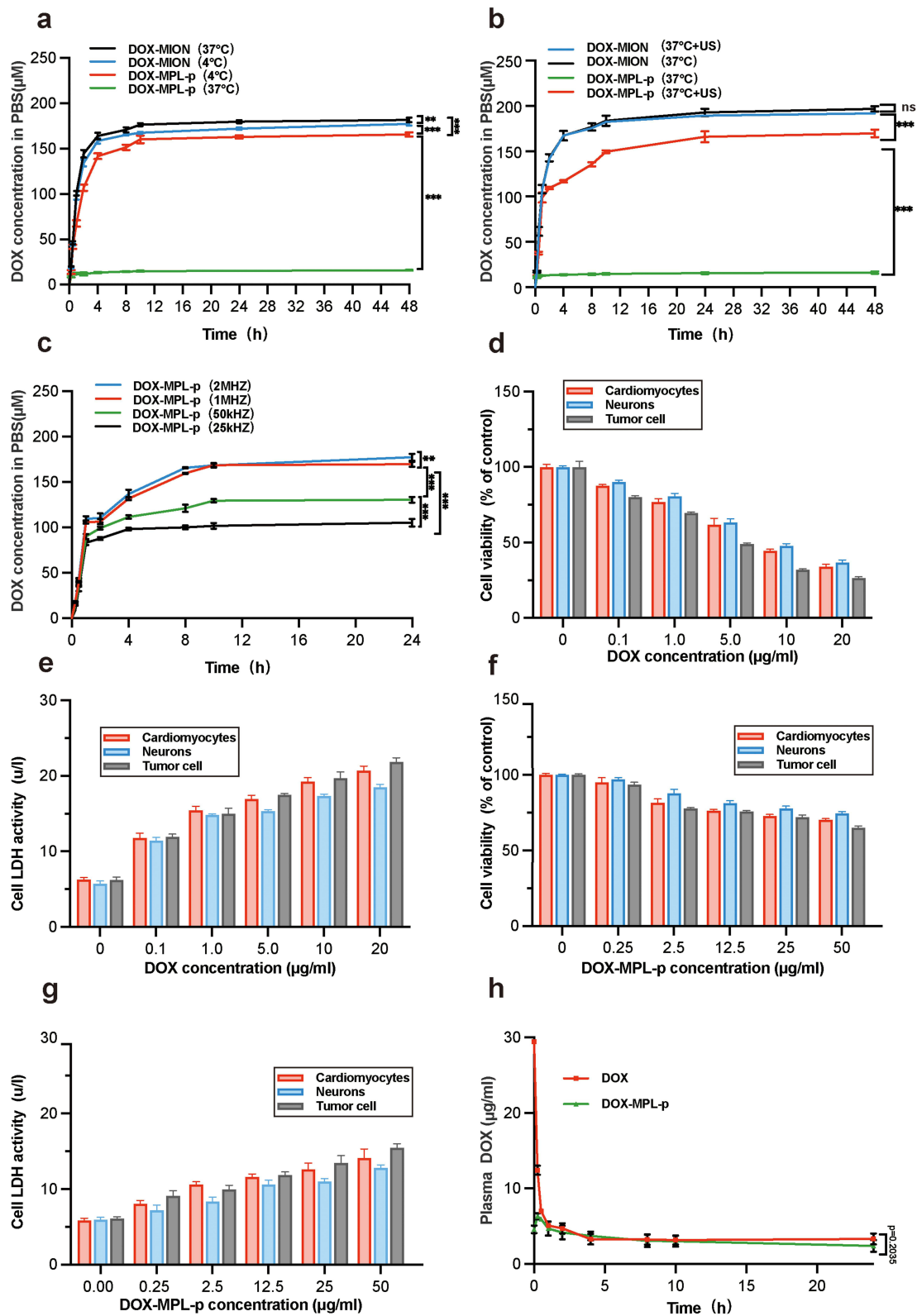


Figure 5 Toxicity assessment and drug release characterization of DOX MPL in vivo and in vitro. Drug release rates of DOX-MPL-p and DOX-MION in vitro at different temperatures (a) and ultrasound-stimulated environment (b); (c) Drug release rates of DOX-MPL-p at different ultrasonic frequencies; Cell viability (d) and lactate dehydrogenase (LDH) activity (e) of cardiomyocytes, neurons and tumor cell after administration of DOX; Cell viability (f) and lactate dehydrogenase (LDH) activity (g) of cardiomyocytes, neurons and tumor cell after administration of DOX-MPL-p; (h) Temporal variations in plasma DOX concentrations of free DOX and DOX-MPL-p post-injection. Asterisks were used to illustrate the level of significance: (***) for $P < 0.001$, (**) for $P < 0.01$, and (ns) for $P > 0.05$.

Biosafety Evaluation

DOX-MPL-p toxicity to various cells was determined by incubating H9C2, PC12, and U87MG cells with the nanoparticles and detecting the cell viability using the CCK-8 assay. Cell viability was significantly decreased at concentrations $> 1 \mu\text{g/mL}$ for all three cell types, and toxicity was the strongest in tumor cells (Figure 5d). The LDH level experiments yielded similar results (Figure 5e). Due to drug release restrictions imposed by the nano gate, DOX-MPL-p exhibited significantly lower toxicity than free DOX, with significantly higher cell viability (Figure 5f). The LDH level experiments yielded similar results (Figure 5g). The *in vivo* drug release profiles of DOX and DOX-MPL-p were obtained by measuring the DOX concentration in plasma (Figure 5h).

The *in vivo* safety was evaluated by injecting DOX-MPL-p (10 mg/kg) into mice via the tail vein. Following administration at 24 h as well as 7, 14, and 21 days, the main mouse organs were obtained and stained using hematoxylin and eosin (H&E). The results revealed that DOX-MPL-p did not cause significant pathological damage. Additionally, the MPL-p regulation of drug release at physiological temperatures substantially reduced its toxic effects: the neuronal cell membranes and soma were intact and neatly arranged; the cardiomyocyte cytoplasm, nuclei, and tissue structures were clear; the hepatic ductal region exhibited normal morphology; the hepatic lobular structure was intact. No obvious abnormalities were observed in the spleen tissues, pulmonary alveolar structures, and renal glomeruli and tubular structures (Figure 6a). Compared to PBS, the heart rate of the mice injected with DOX-MPL-p remained slightly elevated for 16 h (Figure 6b). Although the mean arterial pressure was slightly decreased, it remained within the normal range (Figure 6c). Furthermore, hematological and serological examinations at different time points after drug injection confirmed the biosafety of DOX-MPL-p (Table S1). The biosafety of DOX-MPL-p was also evaluated in an additional experiment last for 3 months, confirming its safety and cardioprotective effects in a long-term and multiple administrations situation (Figure S4).

DOX-MPL-p Alleviate the Drug-Induced Cardiotoxicity in Mice

The survival results demonstrated that the median survival period of the DOX group was 29.5 days, while the DOX-MPL-p group exhibited significantly improved survival (Figure 7a). The administration of free DOX caused cardiac atrophy, which was evaluated using global heart size (Figure 7b) and heart weight/tibia length (Figure 7c), while DOX-MPL-p alleviated these effects. Compared to free DOX, DOX-MPL-p resulted in less cardiac structural and functional damage two weeks after administration (Figure 7d), with more preserved stroke volume (Figure 7e), ejection fraction (Figure 7f), and fraction shortening (Figure 7g).

DOX-MPL-p Demonstrated Superior Organ-Targeting Efficiency

The *in vitro* imaging experiment demonstrated that DiR@MPL-p and DiR@MION exhibited fluorescence at specific wavelengths (Figure S5). The mice were euthanized at 0.5, 4, 8, and 24 h after DiR@MPL-p and DiR@MION injection, and the major organs were acquired for quantitative analysis of fluorescence signals (Figure 8a). At 24 h, the immunofluorescence staining results revealed accumulation of DiR@MPL-p in cerebral cells, while the DiR@MION treatment group had no obvious fluorescent signal in the same area (Figure 8b). The quantitative analysis results demonstrated that DiR@MPL-p mainly accumulated in the liver (Figure 8c) but was also observed in brain tissues 4 h after the injection (Figure 8d). On the contrary, the signal was rarely detected in the brain tissues of the DiR@MION treatment group. The optimal timing of ultrasonic stimulation was determined by applying the stimulation at different times after DOX-MPL-p administration. The drug release experiments revealed that DOX-MPL-p significantly released large amounts of loaded drugs after ultrasonic stimulation in brain tissues (Figure 8e), which was most significant at 4 h of simulation. These findings indicated that the MPL-p released the cargo the brain-targeting capability in response to ultrasonic stimulation.

Discussion

Nanoparticles are widely utilized to improve drug delivery in biomedicine. For example, nanocarriers can target tumor cells and the tumor microenvironment, enhancing drug efficacy and the related treatment effects. These nanocarriers are characterized by their high-drug loading content, good biocompatibility, and slow-release profiles.³¹ However, the current

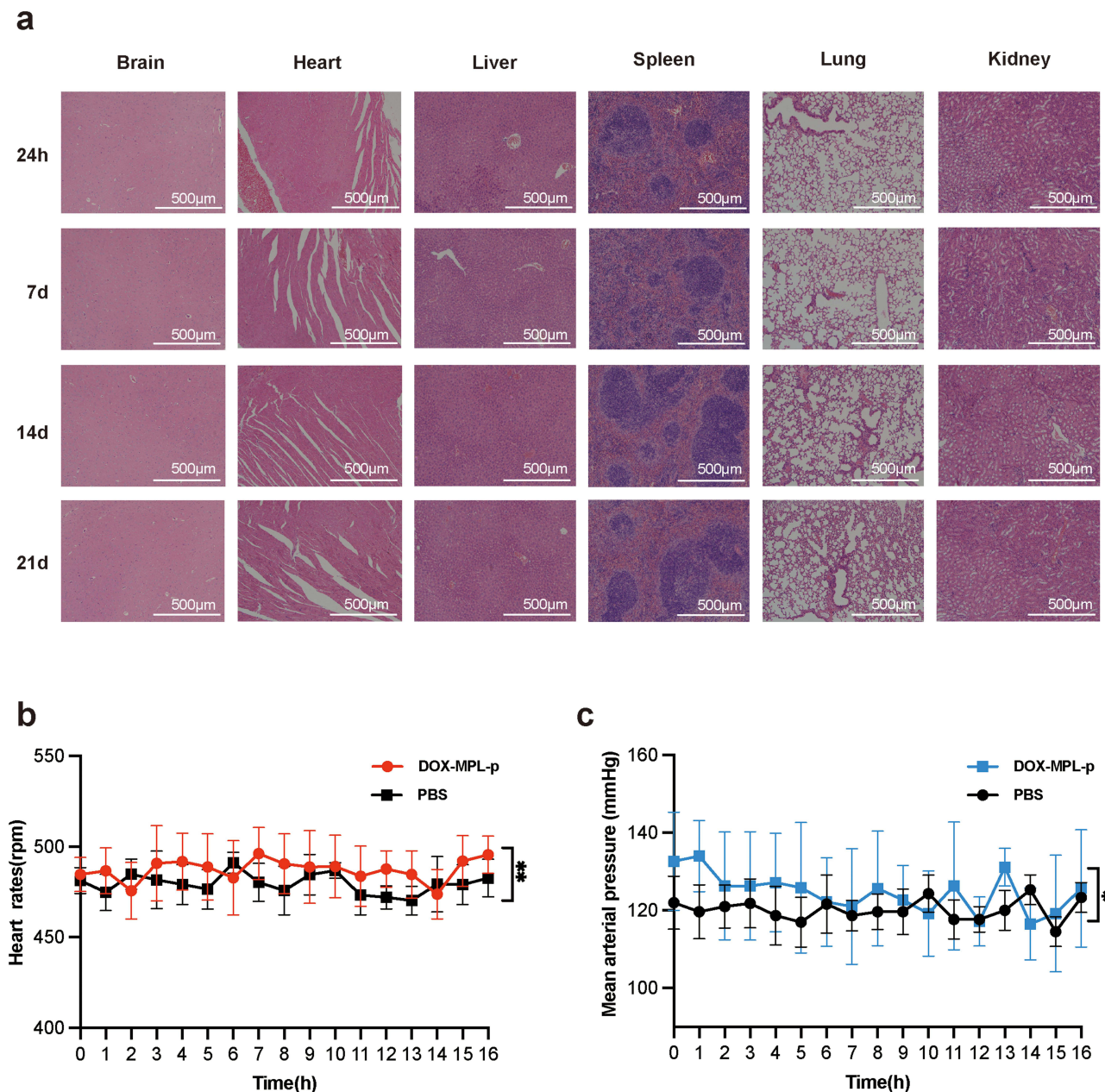


Figure 6 Biosafety of DOX-MPL-p. (a) The H&E staining results of the vital organs of mice injected with DOX-MPL-p observed at 40x magnification, revealed no significant pathological damage. This observation was consistent across various time points: 24 h, 7 d, 14 d, and 21 d post-administration; (b) Heart rates and artery pressures (c) in 16 h after injection. Asterisks were used to illustrate the level of significance: (*) for $P < 0.05$, (**) for $P < 0.01$.

DDS mainly releases drugs in circulation but not in targeted organs, causing suboptimal targeting accuracy. Furthermore, drug release in the bloodstream results in systemic toxicity and non-specific organ accumulation.

Cardiotoxicity is a major concern among the adverse effects caused by drug administration, such as chemotherapy drugs.³² Conventional chemotherapy agents are widely implicated in cardiac dysfunction and heart failure, inhibiting signal transduction by disrupting the cardiac signaling pathways.³³ DOX is a widely used chemotherapy drug and study tool that can significantly trigger oxidative stress, mitochondrial impairment, and subsequent cardiomyocyte apoptosis.³⁴ Other drugs, such as vinblastine and paclitaxel, have been associated with myocardial ischemia and bradycardia,³³ while platinum-based therapies can increase thromboxane levels, contributing to cardiac ischemia.³⁵ The cumulative dosage of these agents is directly linked to cardiotoxicity incidence, and drug overaccumulation in the heart is an independent risk

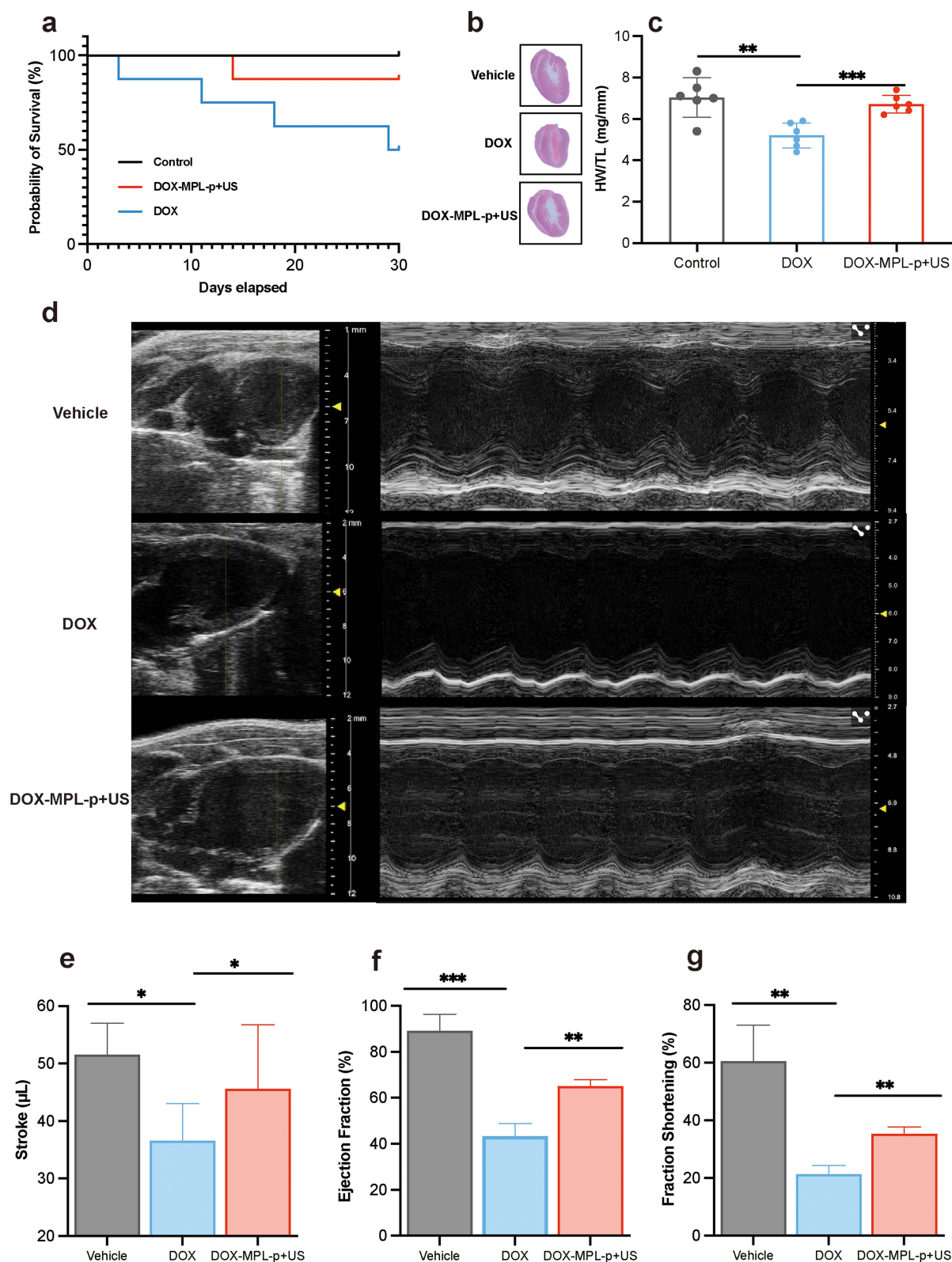


Figure 7 MPL-p reduces the damage of drugs to cardiac function as a DDS. (a) Survival estimates by Kaplan–Meier in Vehicle (PBS), DOX, and DOX-MPL-p treatment groups within 30 d (n = 8); (b) Representation images of H&E staining in mice heart after drug treatment; (c) Quantification of heart weight/tibia length; (d) Representative M-mode echocardiographic images of each group at 14 d point after drug treatment; (e) stroke volume, ejection fraction (f), and fraction shortening (g) measured by echocardiography. Asterisks were used to illustrate the level of significance: (*) for P < 0.05, (**) for P < 0.01, and (***) for P < 0.001.

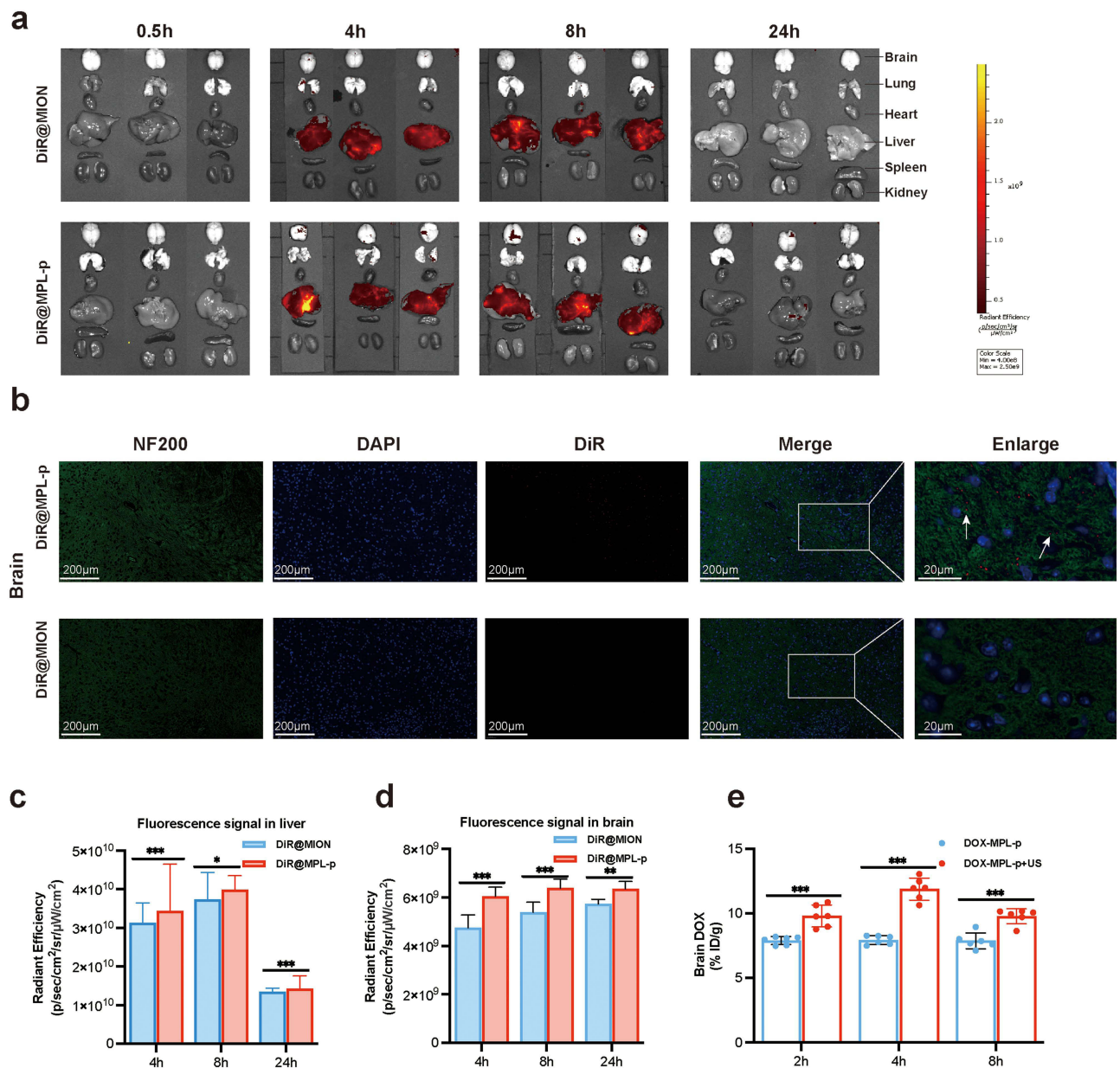


Figure 8 Organ-specific drug release properties of DOX-MPL-p. (a) Fluorescence signals of the brain, heart, liver, spleen, and kidney presented at 0.5 h, 4 h, 8 h, and 24 h after injection of DiR@MPL-p and DiR@MION; (b) Immunofluorescence images of the frozen brain tissues at 24 h after injection of DiR@MPL-p and DiR@MION, and the white arrows indicates the red fluorescent signal emitted by DiR@MPL-p in the brain tissue; Compare the intensity of fluorescence signal in liver (c) and brain (d); (e) The DOX content in the brain tissue by ultrasonic stimulation at 2 h, 4 h, and 8 h after administration of DOX-MPL-p. Asterisks were used to illustrate the level of significance: (*) for $P < 0.05$, (**) for $P < 0.01$, and (***) for $P < 0.001$.

factor for heart failure.²⁶ Therefore, an ideal DDS should scarcely release drugs in circulation, efficiently release drugs in the targeted organs, and exhibit better treatment efficacy. Furthermore, it is extremely important to retain chemotherapy agents in the loaders before reaching the pathological sites, which minimizes chemotherapy-induced cardiotoxicity.

Previously, we developed the drug-loading potential of mesoporous nanoparticles.^{36,37} Among these nanoparticles, MIONs have gained increasing interest due to their unique properties. MIONs exhibit excellent biocompatibility as they are slowly metabolized into ferritin in the liver and have relatively prolonged circulation time.³⁸ Additionally, the hydroxylated surface of MIONs facilitates the grafting of various functional ligands.³⁹ Importantly, magnetic resonance imaging (MRI) tracking demonstrated that the superparamagnetic nature of MIONs allows them to be non-invasive.⁴⁰ Therefore, MIONs can be utilized as an ideal DDS framework. We also previously conjugated LF on the MION surface

to explore the brain-targeting ability of the resultant DDS. We observed significant nanoparticle accumulation in the brain, demonstrating the protective effects of the drug on the ischemic brain.⁴¹ However, the MION-based DDS nevertheless cannot restrict drug release in circulation, resulting in limited drug content in targeted organs with somewhat systemic adverse effects.⁴² Therefore, modified MIONs limiting drug release in the bloodstream, enhancing organ-targeting capability, and improving responsiveness to specific stimuli are still in demand.

Based on the above findings, we engineered the copolymer p-(MEO₂MA-co-THPMA) to endow the MIONs with a dual temperature and ultrasonic response capability. The p-(MEO₂MA) segment is sensitive to temperature fluctuations, retains the copolymer in a hydrophilic conformation, and maintains the open mesoporous structure when the temperature falls below its LCST (37 °C), facilitating drug loading.¹³ Upon entry into the bloodstream, where temperatures exceed the LCST, the p-(MEO₂MA) units transition into a hydrophobic state, resulting in the closure of the mesopores, thereby impeding drug release. Integrating THPMA conferred an ultrasound-responsive property to the polymer. Ultrasonic stimulation cleaves the tetrahydropyranyl groups within the polymer, promoting a conformational shift that reopens the mesoporous structure and facilitates drug release through the nanopores. Ultimately, p-(MEO₂MA-co-THPMA) attachment to MION enabled drug loading at low temperatures and subsequent encapsulation during circulation at 37 °C. Unlike the existing DDS, the integration of temperature and ultrasound dual-responsive copolymers ensures strictly drug encapsulation at physiological temperatures, and immediate release triggered by external stimuli, which enhances both the efficiency and safety of drug application.⁴³

The organ-targeting capabilities of the nanoparticles were enhanced by conjugating the brain-targeting ligand LF to MION via PEG. LF receptors (LFR) was found to be present on endothelial cells of the BBB, as well as on neurons and astrocytes.⁴⁴ Also, Lactoferrin has been widely reported in important studies as the brain-targeting ligand.^{45–47} Facilitated by LFR, LF effectively mediates nanoparticle transport across the BBB to target the brain tissues.^{48,49} Many reports indicated that LF enables nanoparticle crossing of the BBB.⁵⁰ Our findings also demonstrated that LF-modified MIONs accumulated in brain tissue. Moreover, LF demonstrates specific anti-cancer properties that can inhibit tumor growth.^{51,52} The attached PEG molecules improve immune evasion and prolong circulation time in plasma.⁵³ In summary, we synthesized the novel MPL-p DDS [MION-PEG-LF-p-(MEO₂MA-co-THPMA)] as an ideal drug delivery tool.

Anthracycline agents, such as DOX, can damage non-targeted organs. For example, delayed cardiac dysfunction was observed in up to 23% of patients, potentially progressing to systolic heart failure.^{54,55} These risks are directly related to the cumulative intracardiac dose of DOX.⁵⁶ The advantages of MPL-p in terms of brain treatment effects and potential to mitigate cardiac toxicity were validated using DOX as the loaded drug to synthesize DOX-MPL-p. Our findings suggested that effective drug encapsulation significantly reduced DOX cytotoxicity on neural cells and cardiomyocytes. The *in vivo* experiments demonstrated that the drug release from DOX-MPL-p was strictly limited to above the LCST, with rare release at 37 °C, while external ultrasound stimulation effectively reinstated drug release. The nanoparticles demonstrated favorable biocompatibility *in vivo*, with normal organ function and no significant inflammatory response observed over 30 days. The carrier MPL-p significantly reduced the rapid release of DOX in the circulation. Accordingly, DOX-MPL-p greatly reduced the DOX-induced cardiotoxicity and atrophy, improving the survival rate in the mice. Additionally, MPL-p exhibited precise brain-targeting capabilities: MPL-p demonstrated significantly increased cerebral fluorescence compared with nanoparticles not conjugated with LF, indicating nanoparticle accumulation in the brain tissues, while ultrasonic stimulation effectively prompted drug release and enhanced its cerebral treatment effects.

The treatment efficacy of previous DOX donors relies mainly hinges on the drug plasma concentration. However, the rapid plasma release of DOX and its transient tissue presence limits the treatment effects on the intended organs and causes off-target drug damage in cardiac tissues. Nevertheless, DOX-MPL-p greatly enhances the targeting efficacy of DOX along with mitigated adverse effects, especially the cardiotoxicity. Consequently, this novel tool represents a more efficacious and safer modality for DOX administration, suggesting a means of mitigating the inherent cardiac toxicity in drug delivery.

There are still several limitations in the present study. First, the higher dose of DOX-MPL-p was not utilized to confirm our conclusion. However, the dosage we used is consistent with several important studies on DOX treatment, and the dose of 4 mg/kg of DOX contained in DOX-MPL-p can sufficiently cause cardiotoxicity.^{57–59} Meanwhile, compared with same amount of the commonly used dose of DOX, less cardiotoxicity was definitely presented by DOX-MPL-p.

Secondly, we did not evaluate the effectiveness effects in the study for our aiming to explore the cardioprotective effects, however, at the administered dose of DOX-MPL-p, the concentrations of mouse cerebral DOX totally reached to the therapeutic levels for cerebral tumors.^{47,60–62} In future studies, we will evaluate the effectiveness of the novel DDS and explore its cardioprotective effects, perhaps at higher doses. Finally, we only utilized DOX to present the cardioprotective effects of the novel DDS, various drugs should be applied in the future to confirm our conclusion. Anyway, our study presented an ideal drug delivery platform with great potential in designing new DDS, with new insights into more precise and controlled drug delivery.

Conclusion

We reported a MION-based temperature and ultrasound dual-responsive brain-targeting DDS. The system exhibited excellent biocompatibility, controlled release characteristics, and brain-targeting properties. DOX-MPL-p can limit the pre-release of the drug in the bloodstream before targeting the desired location, which reduces drug-induced organ injury, including cardiac damage. After reaching the target organ, ultrasound stimulation triggered drug release, enhancing the therapeutic effects on the brain. The system represents a unique platform for MION-based chemotherapy drug delivery and a novel method to increase cerebral treatment efficiency with reduced cardiac damage, which would greatly benefit patients with tumors.

Data Sharing Statement

All study data, including that analyzed, is available within the published article and its [Supplementary Materials](#).

Ethics Approval and Consent to Participate

All animal experiments conducted in this study were approved by the Institutional Animal Care and Use Committee of the Department of Laboratory Animal Science at Fudan University (Grant No. 20160780A176).

Author Contributions

All authors made a significant contribution to the work reported, whether that is in the conception, study design, execution, acquisition of data, analysis and interpretation, or in all these areas; took part in drafting, revising or critically reviewing the article; gave final approval of the version to be published; have agreed on the journal to which the article has been submitted; and agree to be accountable for all aspects of the work.

Funding

This work was supported by the National Natural Science Foundation of China (82370377, 81601663), Natural Science Foundation of Shanghai (23ZR1408800).

Disclosure

The authors report no conflicts of interest in this work.

References

1. Jensen SA, Day ES, Ko CH, et al. Spherical nucleic acid nanoparticle conjugates as an RNAi-based therapy for glioblastoma. *Sci Transl Med*. 2013;5(209):209ra152. doi:10.1126/scitranslmed.3006839
2. Greish K. Enhanced permeability and retention (EPR) effect for anticancer nanomedicine drug targeting. *Methods Mol Biol*. 2010;624:25–37.
3. Maeda H, Wu J, Sawa T, Matsumura Y, Hori K. Tumor vascular permeability and the EPR effect in macromolecular therapeutics: a review. *J Control Release*. 2000;65(1–2):271–284. doi:10.1016/S0168-3659(99)00248-5
4. Christidi E, Brunham LR. Regulated cell death pathways in doxorubicin-induced cardiotoxicity. *Cell Death Dis*. 2021;12(4):339. doi:10.1038/s41419-021-03614-x
5. Mura S, Nicolas J, Couvreur P. Stimuli-responsive nanocarriers for drug delivery. *Nat Mater*. 2013;12(11):991–1003. doi:10.1038/nmat3776
6. Sirsi SR, Borden MA. State-of-the-art materials for ultrasound-triggered drug delivery. *Adv Drug Deliv Rev*. 2014;72:3–14. doi:10.1016/j.addr.2013.12.010
7. Lapresta-Fernández A, Salinas-Castillo A, Capitán-Vallvey LF. Synthesis of a thermoresponsive crosslinked MEO2MA polymer coating on microclusters of iron oxide nanoparticles. *Sci Rep*. 2021;11(1):3947. doi:10.1038/s41598-021-83608-z

8. Ferjaoui Z, Jamal Al Dine E, Kulmukhamedova A, et al. Doxorubicin-loaded thermoresponsive superparamagnetic nanocarriers for controlled drug delivery and magnetic hyperthermia applications. *ACS Appl Mater Interfaces*. 2019;11(34):30610–30620. doi:10.1021/acsami.9b10444
9. Zhang R, Wang Y, Du FS, et al. Thermoresponsive gene carriers based on poly(ethyleneimine)-graft-poly[oligo(ethylene glycol) methacrylate]. *Macromol Biosci*. 2011;11(10):1393–1406. doi:10.1002/mabi.201100094
10. Qiao S, Wang H. Temperature-responsive polymers: synthesis, properties, and biomedical applications. *Nano Res*. 2018;11(10):5400–5423. doi:10.1007/s12274-018-2121-x
11. Karimi M, Sahandi Zangabad P, Ghasemi A, et al. Temperature-responsive smart nanocarriers for delivery of therapeutic agents: applications and recent advances. *ACS Appl Mater Interfaces*. 2016;8(33):21107–21133. doi:10.1021/acsami.6b00371
12. Bordat A, Boissenot T, Nicolas J, Tsapis N. Thermoresponsive polymer nanocarriers for biomedical applications. *Adv Drug Deliv Rev*. 2019;138:167–192. doi:10.1016/j.addr.2018.10.005
13. Paris JL, Cabañas MV, Manzano M, Vallet-Regí M. Polymer-grafted mesoporous silica nanoparticles as ultrasound-responsive drug carriers. *ACS Nano*. 2015;9(11):11023–11033. doi:10.1021/acsnano.5b04378
14. Wang J, Pelletier M, Zhang H, Xia H, Zhao Y. High-frequency ultrasound-responsive block copolymer micelle. *Langmuir*. 2009;25(22):13201–13205. doi:10.1021/la9018794
15. Kumari S, Ahsan SM, Kumar JM, Kondapi AK, Rao NM. Overcoming blood brain barrier with a dual purpose temozolomide loaded lactoferrin nanoparticles for combating glioma (SERP-17-12433). *Sci Rep*. 2017;7(1):6602. doi:10.1038/s41598-017-06888-4
16. Owens Iii DE, Peppas NA. Opsonization, biodistribution, and pharmacokinetics of polymeric nanoparticles. *Int J Pharm*. 2006;307(1):93–102. doi:10.1016/j.ijpharm.2005.10.010
17. Dosio F, Arpicco S, Brusa P, Stella B, Cattel L. Poly(ethylene glycol)-human serum albumin-paclitaxel conjugates: preparation, characterization and pharmacokinetics. *J Control Release*. 2001;76(1–2):107–117. doi:10.1016/S0168-3659(01)00420-5
18. Kim SY, Shin IG, Lee YM. Amphiphilic diblock copolymeric nanospheres composed of methoxy poly(ethylene glycol) and glycolide: properties, cytotoxicity and drug release behaviour. *Biomaterials*. 1999;20(11):1033–1042. doi:10.1016/S0142-9612(98)00249-X
19. Kim SY, Lee YM, Baik DJ, Kang JS. Toxic characteristics of methoxy poly(ethylene glycol)/poly(epsilon-caprolactone) nanospheres; in vitro and in vivo studies in the normal mice. *Biomaterials*. 2003;24(1):55–63. doi:10.1016/S0142-9612(02)00248-X
20. Xue W, Liu Y, Zhang N, et al. Effects of core size and PEG coating layer of iron oxide nanoparticles on the distribution and metabolism in mice. *Int J Nanomed*. 2018;13:5719–5731. doi:10.2147/IJN.S165451
21. Lawrence PB, Price JL. How PEGylation influences protein conformational stability. *Curr Opin Chem Biol*. 2016;34:88–94. doi:10.1016/j.cbpa.2016.08.006
22. Hsu HJ, Han Y, Cheong M, Král P, Hong S. Dendritic PEG outer shells enhance serum stability of polymeric micelles. *Nanomedicine*. 2018;14(6):1879–1889. doi:10.1016/j.nano.2018.05.010
23. van der Zanden SY, Qiao X, Neeffes J. New insights into the activities and toxicities of the old anticancer drug doxorubicin. *Febs j*. 2021;288(21):6095–6111. doi:10.1111/febs.15583
24. Pugazhendhi A, Edison T, Velmurugan BK, Jacob JA, Karuppusamy I. Toxicity of Doxorubicin (Dox) to different experimental organ systems. *Life Sci*. 2018;200:26–30. doi:10.1016/j.lfs.2018.03.023
25. Lotrionte M, Biondi-Zoccai G, Abbate A, et al. Review and meta-analysis of incidence and clinical predictors of anthracycline cardiotoxicity. *Am J Cardiol*. 2013;112(12):1980–1984. doi:10.1016/j.amjcard.2013.08.026
26. Swain SM, Whaley FS, Ewer MS. Congestive heart failure in patients treated with doxorubicin: a retrospective analysis of three trials. *Cancer*. 2003;97(11):2869–2879. doi:10.1002/cncr.11407
27. Wouters KA, Kremer LC, Miller TL, Herman EH, Lipshultz SE. Protecting against anthracycline-induced myocardial damage: a review of the most promising strategies. *Br J Haematol*. 2005;131(5):561–578. doi:10.1111/j.1365-2141.2005.05759.x
28. Octavia Y, Tocchetti CG, Gabrielson KL, Janssens S, Crijns HJ, Moens AL. Doxorubicin-induced cardiomyopathy: from molecular mechanisms to therapeutic strategies. *J Mol Cell Cardiol*. 2012;52(6):1213–1225. doi:10.1016/j.yjmcc.2012.03.006
29. Wang W, Liu H, Lu Y, et al. Controlled-releasing hydrogen sulfide donor based on dual-modal iron oxide nanoparticles protects myocardial tissue from ischemia-reperfusion injury. *Int J Nanomed*. 2019;14:875–888. doi:10.2147/IJN.S186225
30. Sun X, Wang W, Dai J, et al. A long-term and slow-releasing hydrogen sulfide donor protects against myocardial ischemia/reperfusion injury. *Sci Rep*. 2017;7(1):3541. doi:10.1038/s41598-017-03941-0
31. Sifaka PI, Üstündağ Okur N, Karavas E, Bikiaris DN. Surface modified multifunctional and stimuli responsive nanoparticles for drug targeting: current status and uses. *Int J Mol Sci*. 2016;17(9):1440. doi:10.3390/ijms17091440
32. Ferri N, Siegl P, Corsini A, Herrmann J, Lerman A, Benghozi R. Drug attrition during pre-clinical and clinical development: understanding and managing drug-induced cardiotoxicity. *Pharmacol Ther*. 2013;138(3):470–484. doi:10.1016/j.pharmthera.2013.03.005
33. Suter TM, Ewer MS. Cancer drugs and the heart: importance and management. *Eur Heart J*. 2013;34(15):1102–1111. doi:10.1093/eurheartj/ehs181
34. Geisberg CA, Sawyer DB. Mechanisms of anthracycline cardiotoxicity and strategies to decrease cardiac damage. *Curr Hypertens Rep*. 2010;12(6):404–410. doi:10.1007/s11906-010-0146-y
35. Iorio-Morin C, Germain P, Roy S, Génier S, Labrecque P, Parent JL. Thromboxane A2 modulates cisplatin-induced apoptosis through a Siva1-dependent mechanism. *Cell Death Differ*. 2012;19(8):1347–1357. doi:10.1038/cdd.2012.11
36. Sun X, Kong B, Wang W, et al. Mesoporous silica nanoparticles for glutathione-triggered long-range and stable release of hydrogen sulfide. *J Mater Chem B*. 2015;3(21):4451–4457. doi:10.1039/C5TB00354G
37. Wang W, Sun X, Zhang H, et al. Controlled release hydrogen sulfide delivery system based on mesoporous silica nanoparticles protects graft endothelium from ischemia-reperfusion injury. *Int J Nanomed*. 2016;11:3255–3263. doi:10.2147/IJN.S104604
38. Raynal I, Prigent P, Peyramaure S, Najid A, Rebuzzi C, Corot C. Macrophage endocytosis of superparamagnetic iron oxide nanoparticles: mechanisms and comparison of ferumoxides and ferumoxtran-10. *Invest Radiol*. 2004;39(1):56–63. doi:10.1097/01.rli.0000101027.57021.28
39. Huang G, Zhang C, Li S, et al. A novel strategy for surface modification of superparamagnetic iron oxide nanoparticles for lung cancer imaging. *J Mater Chem*. 2009;19(35):6367–6372. doi:10.1039/b902358e
40. Semelka RC, Helmlinger TK. Contrast agents for MR imaging of the liver. *Radiology*. 2001;218(1):27–38. doi:10.1148/radiology.218.1.r01ja2427
41. Sun X, Wang Y, Wen S, et al. Novel controlled and targeted releasing hydrogen sulfide system exerts combinational cerebral and myocardial protection after cardiac arrest. *J Nanobiotechnol*. 2021;19(1):40. doi:10.1186/s12951-021-00784-w

42. Wang S, He H, Mao Y, Zhang Y, Gu N. Advances in atherosclerosis theranostics harnessing iron oxide-based nanoparticles. *Adv Sci*. 2024;11(17):e2308298. doi:10.1002/advs.202308298
43. Matanović MR, Kristl J, Grabnar PA. Thermoresponsive polymers: insights into decisive hydrogel characteristics, mechanisms of gelation, and promising biomedical applications. *Int J Pharm*. 2014;472(1–2):262–275. doi:10.1016/j.ijpharm.2014.06.029
44. Qian ZM, Li W, Guo Q. Lactoferrin/lactoferrin receptor: neurodegenerative or neuroprotective in Parkinson's disease? *Ageing Res Rev*. 2024;101:102474. doi:10.1016/j.arr.2024.102474
45. Fang JH, Chiu TL, Huang WC, et al. Dual-targeting lactoferrin-conjugated polymerized magnetic polydiacetylene-assembled nanocarriers with self-responsive fluorescence/magnetic resonance imaging for in vivo brain tumor therapy. *Adv Healthc Mater*. 2016;5(6):688–695. doi:10.1002/adhm.201500750
46. Tang S, Wang A, Yan X, et al. Brain-targeted intranasal delivery of dopamine with borneol and lactoferrin co-modified nanoparticles for treating Parkinson's disease. *Drug Deliv*. 2019;26(1):700–707. doi:10.1080/10717544.2019.1636420
47. Zhang M, Asghar S, Tian C, et al. Lactoferrin/phenylboronic acid-functionalized hyaluronic acid nanogels loading doxorubicin hydrochloride for targeting glioma. *Carbohydr Polym*. 2021;253:117194. doi:10.1016/j.carbpol.2020.117194
48. Huang R, Ke W, Han L, et al. Brain-targeting mechanisms of lactoferrin-modified DNA-loaded nanoparticles. *J Cereb Blood Flow Metab*. 2009;29(12):1914–1923.
49. Zhao C, Zhang J, Hu H, et al. Design of lactoferrin modified lipid nano-carriers for efficient brain-targeted delivery of nimodipine. *Mater Sci Eng C Mater Biol Appl*. 2018;92:1031–1040. doi:10.1016/j.msec.2018.02.004
50. Tang J, Bian Z, Hu J, Xu S, Liu H. The effect of a P123 template in mesopores of mesocellular foam on the controlled-release of venlafaxine. *Int J Pharm*. 2012;424(1–2):89–97. doi:10.1016/j.ijpharm.2011.12.048
51. Zhang Y, Lima CF, Rodrigues LR. Anticancer effects of lactoferrin: underlying mechanisms and future trends in cancer therapy. *Nutr Rev*. 2014;72(12):763–773. doi:10.1111/nure.12155
52. Cutone A, Colella B, Pagliaro A, et al. Native and iron-saturated bovine lactoferrin differently hinder migration in a model of human glioblastoma by reverting epithelial-to-mesenchymal transition-like process and inhibiting interleukin-6/STAT3 axis. *Cell Signal*. 2020;65:109461. doi:10.1016/j.cellsig.2019.109461
53. Knop K, Hoogenboom R, Fischer D, Schubert US. Poly (ethylene glycol) in drug delivery: pros and cons as well as potential alternatives. *Angew Chem Int Ed*. 2010;49(36):6288–6308. doi:10.1002/anie.200902672
54. Cardinale D, Colombo A, Lamantia G, et al. Anthracycline-induced cardiomyopathy: clinical relevance and response to pharmacologic therapy. *J Am Coll Cardiol*. 2010;55(3):213–220. doi:10.1016/j.jacc.2009.03.095
55. Steinherz LJ, Steinherz PG, Tan CT, Heller G, Murphy ML. Cardiac toxicity 4 to 20 years after completing anthracycline therapy. *JAMA*. 1991;266(12):1672–1677. doi:10.1001/jama.1991.03470120074036
56. Shan K, Lincoff AM, Young JB. Anthracycline-induced cardiotoxicity. *Ann Intern Med*. 1996;125(1):47–58. doi:10.7326/0003-4819-125-1-199607010-00008
57. Kong CY, Guo Z, Song P, et al. Underlying the mechanisms of doxorubicin-induced acute cardiotoxicity: oxidative stress and cell death. *Int J Biol Sci*. 2022;18(2):760–770. doi:10.7150/ijbs.65258
58. Hu C, Zhang X, Song P, et al. Meteorin-like protein attenuates doxorubicin-induced cardiotoxicity via activating cAMP/PKA/SIRT1 pathway. *Redox Biol*. 2020;37:101747. doi:10.1016/j.redox.2020.101747
59. Wang AJ, Tang Y, Zhang J, et al. Cardiac SIRT1 ameliorates doxorubicin-induced cardiotoxicity by targeting sestrin 2. *Redox Biol*. 2022;52:102310. doi:10.1016/j.redox.2022.102310
60. Peter S, Alven S, Maseko RB, Aderibigbe BA. Doxorubicin-based hybrid compounds as potential anticancer agents: a review. *Molecules*. 2022;27(14):4478. doi:10.3390/molecules27144478
61. Liu G, Tsai HI, Zeng X, et al. Phosphorylcholine-based stealthy nanocapsules enabling tumor microenvironment-responsive doxorubicin release for tumor suppression. *Theranostics*. 2017;7(5):1192–1203. doi:10.7150/thno.17881
62. Cen J, Dai X, Zhao H, et al. Doxorubicin-loaded liposome with the function of “killing two birds with one stone” against glioma. *ACS Appl Mater Interfaces*. 2023;15(40):46697–46709. doi:10.1021/acsmi.3c10364